Spring 5-2017

Stabilization of Iron Oxide Nanoparticles for Homogenous Integration Into Cellulose Nano Fibrils

Banton H. Heithoff
University of Maine

STABILIZATION OF IRON OXIDE NANOPARTICLES FOR HOMOGENOUS INTEGRATION INTO CELLULOSE NANO FIBRILS

By

Banton H Heithoff

A Thesis Submitted in Partial Fulfillment of Requirements for a Degree with Honors (Bioengineering)

The Honors College

University of Maine

May 2017

Advisory Committee:

Michael D. Mason, Professor of Chemical and Biological Engineering, Advisor

Ian Dickey M.D., Adjunct Faculty Chemical and Biological Engineering

Mehdi Tajvidi, Assistant Professor of Renewable Nanomaterials

Rosemary Smith, Professor of Electrical and Computer Engineering

François G. Amar, Professor of Chemistry and Dean of the Honors College

Abstract

Cellulose nanofibrils is one of the future potential giants in the medical implant industry. Its unique properties make it the ideal material for use in both permanent prosthetic devices and non-permanent implants such as screws and plates. To increase the usability of this material, the addition of super paramagnetic iron oxide nanoparticles is needed to gain MRI and X-Ray visibility. The methodology for how to homogenously integrate these particles into the system using the addition of coating agents is explored. This research demonstrates that the addition of coating agents to the iron oxide nanoparticles can affect both the pH flocculation behavior and the adhesion of the particles to fibrils. In addition, the research finds that the addition of coating agents affects the physical characteristics of the fibrils themselves.

Acknowledgements

I would like to thank the entire Mason Lab for their assistance in both research methodology and the writing process. Special thanks to David Holomakoff and Ratawan Hossen who acted as constant sources of information through the project. In addition, I would like to thank family and friends for continued support throughout my collegiate carrier as well as during this project. Final Thanks go to Dr. Michael Mason for his guidance.

Table of Contents

Appendix A Figures

Appendix B Tables

Background of Medical implants

In the ever-advancing field of medical implants, both temporary devices and more permanent inserts, there is a pressing need for more biologically suited materials. Current medical implants are commonly made of cobalt-chromium-molybdenum or titanium alloys among others. (3) These materials are great at absorbing external forces and have been critical in the success of implants throughout the past century. (3) There are three major problems with current medical implants; elastic moduli that are ill suited for biological contexts, the inability for implants to be integrated into surrounding biological tissues or completely resorbed, and the challenges that arise when attempting to image the implants with x-ray and magnetic resonance imaging (MRI).

The vastly different elastic modulus of the metal implants is the underlying cause of the metal implants' biggest drawback, aseptic loosening. Aseptic loosening is a process by which the implants become loosened by movement of the implant inside of the body. Aseptic loosening is the number one cause of medical implants failure.(4) These movements are due to the bone failing to regrow properly and integrate with the implant. This then leads to a loss in the cortical density of the bone surrounding the implant. (5) One of the current goals of medical implant research is to incorporate a design feature into the device which would allow for bone to grow into the system. This would not only assist with preventing rejection but better facilitate the healing process. One established method for accomplishing this goal is to incorporate a porous external structure that bone naturally is able to grow into. (6) Other attempts have been made to use Hydroxyapatite as a coating on the surface of the implant to encourage regrowth. While these methods have been proven somewhat successful they also add an additional step to the implantation manufacturing process. (7) These added steps increase both the complexity of the device, which increases the risk of mechanical failure and the cost of the devices. These challenges are not unique to permanent

implants. Medical screws, plates, and pins suffer from the same difficulties. Plates and screws often need to be removed after they have served their usefulness in order to facilitate proper healing. (8)

Along with integration of the implant with the surrounding tissues, one possible goal of medical implants is the complete resorption of the device into the body. This process allows for implant devices to be completely taken up by the surrounding tissues preventing the need for removal later either by design, to complete healing processes, or to correct a damaged device. Conventional metal implants cannot be taken up by the body by design, these materials are often toxic and if they are absorbed lead to health complications.(9) Current devices designs are attempting to address this problem using magnesium based implants which, through design controls, allow for slow absorption of the implant. This is not a perfect solution however as they require a subcutaneous needle at the implant site to vent off hydrogen gas that is being produced in the decomposition and have variable break down times due to, "increased acidity in the environment of some fractures."(10) The combination of a continuous port for possible infection and difficulty in controlling degradation make use of magnesium implants a daunting challenge in medical practice. Resorbable materials are not limited to metals. Polymers such as BioSorbFX and LactroSorb are being used to make resorbable screws. These devices while promising but still have difficulties with inflammation and monitoring through imaging, being completely transparent to standard techniques. (8)

In addition to struggling to integrate the bone tissue into the structure of the implant, another cause of aseptic loosening is failure to allow the surrounding bone to retain the natural force loads that are necessary for bones to retain their strength and functionality. (11) The implants take much of the forces of day to day life because of significant differences in the elastic modulus

of the material. Common materials for implants have ratings' from 110 – 230 GPa. This elastic modulus is an order of magnitude higher than that of normal human cortical bone which ranges from 10-30 GPa. Seeing this difference in mechanical properties and the problems that it causes a new generation of titanium alloys having elastic modulus 74-85 GPa. (3) Despite the efforts to the replications of the innate mechanical properties the elastic moduli still dramatically exceed that of normal bone and do not eliminate the complications.

Medical implants need to be monitored during their time in-vivo to both ensure that the material is not leaching in the body and to monitor the physical condition of the implant. Classical metal implants can be monitored through non-invasive techniques such as x-rays or MRI's. While metal implants are capable of being imaged using these technologies due to the nature of the material, they are susceptible to image distortion leading to difficulties in monitoring.(12) Polymeric implants are radiolucent and cannot be imaged by these methods. Consequently, if a possible problem arises the implant needs to be visually inspected through surgical procedures. For implants that are designed to biodegrade the monitoring of integration of osteocytes is done indirectly by watching the screw sites. (8) The future of polymeric implants is dependent on the development of technologies that allow for their imaging.

Introduction

One obvious solution to the problems facing medical implants is to use real bone in the implants. This would prevent all material based rejection issues as prevent complications caused by the differences in the elastic modulus. Unfortunately, synthetic bone is not available. A potentially-viable alternative is the mimicry of the cellular component of bone, the collagen, using cellulose nano-fibrils (CNF). The cellulose and the collagen fibers have similar mechanical properties.(13) Cellulose is one of the most plentiful polymers in nature as it is the primary reinforcement structure in plants as well as few bacteria. Critically cellulose has been shown to be biocompatible making it a viable option for in-vivo implantation. (14)

The ubiquity of CNF is not an indicator of simplicity, Cellulose is an organic non branched polymer chain that contains "1–4-linked β-d-anhydroglucopyranose units". (1)(15) It is extracted from wood and depending on the source material can have variable chain lengths. (1)(15) In addition to source determining the chain length the diameter of the native cellulose fiber, varying from 2.5nm to tens of nanometers is also affected. (15)(16) Along the length of the chains, hydroxyl groups preform intra and intermolecular hydrogen bonding. These bonds allow the cellulose polymers to be grouped together in highly complex crystalline structures. The collagen polymers are arranged in units called micro-fibrils. The prefix micro is a nomenclature error and does not reflect the scale of the fibers (1) as the fibers themselves are on the order of nanometers and add to the strength and versatility of the structure.

Once the wood products have been processed, these cellulose microfibrils can be isolated. Fibril aggregates with diameters below 100 nm are produced by subjecting them to high shear forces in a homogenizer. Once this process is complete, the material now falls under the classification of cellulose nanofibrils. (1) The finished CNF is a slurry mixture, the fibrils being

suspended in water. CNF is highly hydrophilic making it an ideal material to combine with other hydrophilic compounds. These fibrils are an ideal medium to work with because of their, "high strength and stiffness combined with low weight, biodegradability, and renewability." (15) Another advantageous characteristic of the cellulose is its native porous structure, a large contributor to its high strength to weight ratio. These pores are a critical feature of CNF that can be exploited in medical devices allowing for tissues to interpenetrate into the structure without any complicated modification to the structure. In addition to being part of the native structure, the size of the pore is highly tunable by variations in the method of drying. (17)

One of cellulose's difficulties in the medical implant field is that it is undetectable by X-rays and MRI. This is due to the lack of the mineral hydroxyapatite found in bone which provides the dense media for with the X-rays or radio waves to interact with in the body. (18)(12) This results in a limitation of use because if there is a problem, or suspected problem with the cellulose based implant, the only truly diagnostic procedure to assess the situation is via invasive surgery. This limitation is shared by the polymeric implants and is one of the key challenges that must be overcome for their expanded use.

One proposed method for adding the MRI and X-ray contrast is the addition of superparamagnetic iron oxide nano-particles to the cellulose fibrils.(19) There are two variants of iron oxide nano-particles, Fe_2O_3 and Fe_3O_4, the due to the ease of use and synthesis of the particle the Fe_2O_3 variety will be used. The superparamagnetic nature of the Nano-particles grant them the ability to be seen by MRI, and the iron content of the particles allow them to be imaged through X-rays. (12)(18) superparamagnetic particles are characterized by their size which has to be below 20 nm. This size causes the particles to have enhanced interaction with protons.(20) These particles are a not only superparamagnetic but super hydrophilic; the particles are suspended in water after

the synthesis and once in solution, they remain stable in solution for years as shown by the samples prepared in the Mason lab. Despite their high stability and hydrophilicity, the particles flocculate under biological conditions, most notable biological pH's.

The native particles have a pH once produced of near 2.5, this low pH puts the particles in a safe zone far from the isoelectric point of pH 7. As the particles approach the isoelectric point

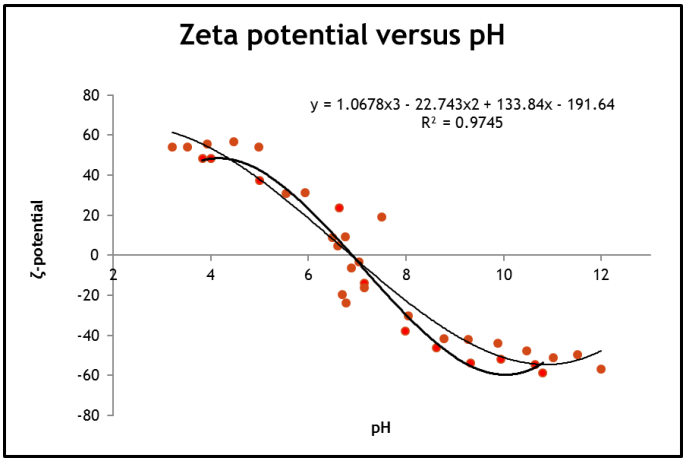

Figure 1 Zeta potential Curves of Naked Fe2O3

the electrostatic repulsion between the particles can no longer stabilize the particles and they flocculate out of the solution. The electrostatic stability is quantified through the zeta-potential of the particles. Zeta potential is caused by the accumulation of charges around the surface of the particle the larger the value the higher level of stability to the colloidal system. (21) At the native reactor pH of 2.5, the particles zeta-potential is consistently at 60 mV; this high zeta-potential creates a high level of stability due to the electrostatic forces found between each of the particles. In addition, highly alkaline pH's grant similar stability with the Zeta potential being -60mV. As the system approaches a pH of seven the zeta-potential reaches zero removing the electrostatic stability from the system and the particles flocculate. (Figure 1)

To overcome the lack of electrostatic stabilization steric stabilization is being explored. To increase the steric stability of the particles an external agent will need to be added to the surface of the particles. Two different groups of polymers were selected; polyethylene glycol and cellulosic polymers. All the polymers utilize the same mechanism to increase the colloidal stability, the polymer will bind at the surface of the particle and the remainder of the chain will reach out into the inter-colloidal space. These chains of polymers act by physical means to keep the particles from achieving flocculation. There are two major processes by which the polymers can be added to the surface of the particles: Physisorption for polyethylene glycol molecules and chemisorption for cellulosic polymers. Physisorption is the process by which the polymers can bond to the surface of the particles by Van der Waals interactions. These are weak interactions typically having binding energies between 5-50 kJ/mol. (21) These are non-permanent interactions and do not react with the particles in a classical sense and consequently low amounts of energy are required to achieve binding, making the reaction rapid and easily achieved.(22)

Chemisorption is a more energetic form of surface adsorption. The surface of the iron oxide particles is covered in oxygen molecules and thus is highly susceptible to hydrogen bonding. It is through this hydrogen bonding that the cellulosic polymers (Dextran, Galactose, and Xylose) are able to bind. (19) Unlike the physisorption mechanism, this is permanent interaction and thus has a much higher energy requirement (50-500 kJ/mole); these higher energies make it so the coating process takes longer to reach completion. (21)

To quantify the quality of bot the particle stabilization and integration into the cellulose five methods of data analysis are used to quantify the particle system: UV-Vis spectroscopy, Dynamic Light Scattering (DLS), zeta-potential analysis, scanning electron microscopy (SEM), and Fourier Transformed Infrared Spectroscopy (FTIR). The particles in a water suspension will

be characterized using UV-Vis, DLS, and zeta-potential analysis to ensure the quality of the particles and choose the particle and coating agents to be integrated into the cellulose fibrils. Once the particles have been integrated into the fibrils the quality of integration will be determined qualitatively by SEM and quantitatively by FTIR.

UV-Vis spectroscopy is used to quantify the particle flocculation in solution. The device used in these experiments is Ocean Optics USB4000. The device works by emitting a beam of light, 178 nm to 890 nm, covering both the near ultra violet and visible spectrums of light. The light then interacts with the sample and causes the photons at given wave lengths to be absorbed

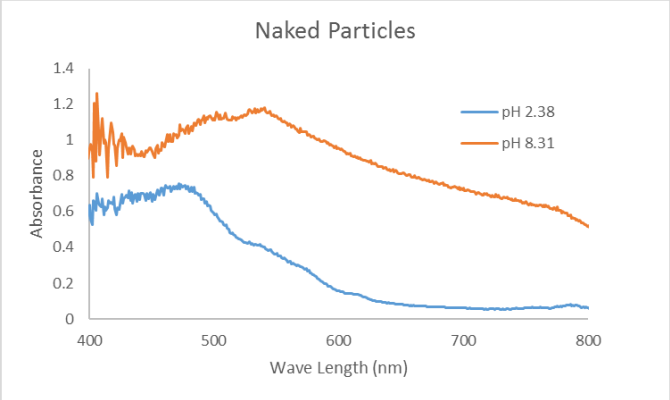

Figure 2 Naked Fe2O3 UV-Vis Spectra Pre-and Post Flocculation

by the sample. The wave lengths that are absorbed are characteristic of the material that is being analyzed. The light traverses a known path length. Using the ratio of the intensities and Beer's Law, the concentration of the solution can be determined. In addition to the wavelengths, the concentration, and opacity of the sample affect the spectral results. The instrument reads the optical density by calculating how much of the initial intensity of light passes through the solution. If the solution is too concentrated or is opaque, UV-Vis spectroscopy cannot be used because not enough light can pass through the sample. (23) Iron oxide nano-particle have an absorbance peak of 450 nm with a bandwidth of 200 nm. When the particles flocculate, the absorbance peak shifts right to

530 nm and the bandwidth increase to 476 nm. Therefore, the stock solution of the particles needs to be adjusted to achieve viable results as stock solutions are completely unpassable to light due the high density of particles, at 0.0125 gm/mL. To standardize the absorbance for multiple experiments an absorbance value of one is selected. To achieve this value, a final particle concentration of $1.25*10^{-4}$ gm/mL is required.

To determine the size and distribution of particle systems dynamic light scattering (DLS) is needed. For these experiment, a zeta sizer nano series by Malvern instruments was used. Dynamic light scattering uses the subtle motion of particles in solution called Brownian motion, which is dependent both on the material being analyzed and the solvent, to find the size of particles. The instrument sends light into the sample and the particle suspension scatters the light. As the measurements are being made the particles continue to fluctuate in position. These fluctuations are time dependent. Given their location, it changes the amount of light being scattered by either constructive or destructive interference. These fluctuations are then correlated to a decay rate which can then be related to the diffusion rate. This diffusion rate can then be used in Stokes-Einstein equation to calculate the hydraulic diameter. (24) The sizes and distributions of the particles are recorded for the initial record conditions to ensure the viability of the particle batch as well as at critical points during zeta potential sweeps.

To calculate the electrostatic stabilization and isoelectric point of the solution the Zeta Sizer Nano series by Malvern instruments is used, the same instrument used for DLS measurements. Zeta potential is the measure of net electrical charge of the surface layer of particles. Around the surface of particles three distinct layers of charge exist; the surface charge, stern charge, and the zeta potential; this final layer correlates to the slipping plane of the particle. This slipping plane is the outer most layer of charge influence on the fluid surrounding the particle. The sample is

introduced into the instrument and an electric charge is placed across the solution. This causes the particles to migrate via electrophoresis motility in the direction of the opposite charge. Different zeta potentials of the particles cause variance in the rate the particles migrate. As the particles move the instrument passes light through the solution of known intensity and wave length. As the light interacts with the particle solution the slight scatters, due to the motion of the particles, both electrophoresis as well as Brownian motion, the scatter light experiences Doppler shifting. The Doppler shifting is then used to calculate the zeta potential through use of the Smoluchowski equation. (21)

Once the particles have been added into the fibrils they need to be examined for the quality of the integration. A qualitative analysis of particle coverage of the fibrils is best preformed through visual inspection. Because of the small size of fibrils and particles, the only way to achieve a high enough resolution is through transmission electron microscopy (TEM) or scanning electron microscopy (SEM) imaging. The use of electrons as the beam source, as opposed to light is needed because of the resolution requirements; light is limited to 0.2 microns while electrons are capable of resolutions of 25 Å. Due to the samples being suspend in a three-dimensional dried matrix TEM is not the proper instrument to use. The SEM, however, provide a better view of three dimension as well as works well on dried material. The SEM works by generating and focusing an electron beam under vacuum conditions. Then by using electromagnetic deflection coils, the beam is passed over the surface of the material. The imaging of the surface exploits two different phenomena to achieve their images: secondary and backscattered electrons. Secondary electrons result from the inelastic collisions and grant resolution of 10 nm. Backscattered electrons are a consequence of elastic collisions and scattering of the incident electrons and the material being scanned. The backscattered electrons are used in resolving the surface topography of the specimen. (25)

In addition to a qualitative analysis of the fibers coating of the surface a quantitative analysis is needed. The method chosen is Fourier transformed infrared spectroscopy (FTIR). This method is one of the analytical standards and has a long history of being used for study of cellulose fibrils. (26) This method utilizes the resultant intermolecular motion of atoms when they are exposed to infrared light. There are three types of motion that molecules can experience, vibration, bending, and stretching, each giving a unique FTIR energy signature. When bonds are exposed to light energy a fraction of the energy is absorbed, the level of energy is dependent on the type of bond and the location of the bond in the molecule. In Attenuated Total Reflectance (ATR) uses the phenomenon of total internal reflection. As the beam of light passes through the crystal, the beam interacts with the surface layer of the material that is in contact with the crystal. As the material interacts, it loses energy in discrete quantities. From the remaining energies, a spectrum is created and represents a fingerprint for each individual molecule and structure.(27) The structure

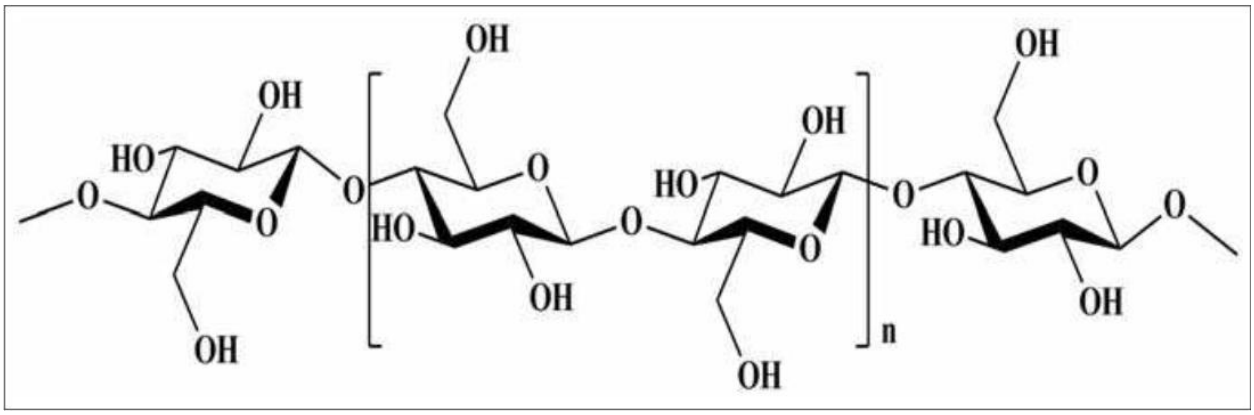

Figure 3 Cellulose Structure (26)

of cellulose (Figure 3) grants a variety of sites for FTIR signals. The selected region of stretching used to quantify is a peak of 1506 cm^{-1}, this peak corresponds to C=C aromatic symmetrical stretching. This region is chosen because of its location and its strong signal. (26) The location is important because the signal is far from the peaks of the iron oxide, two peaks found between 450 cm^{-1} and 560 cm^{-1} (28). The strength of the peak is also important as the goal is to correlate the

degree of coverage of the particles on the cellulose fibrils to the intensity of the peak. Initial attempts to take the spectra of the cellulose fibers were met with two challenges. First, the background spectra from the air makes it difficult to discern the peaks of the cellulose. To solve this problem, the FTIR underwent a Nitrogen gas purge to remove the ambient gases. The second challenge arose due to the nature of the dried CNF. That is, the CNF dries in irregular shapes which make it difficult to have it evenly and reliably pressed against the surface of the crystal. Despite the complications of this drying method this methodology was used due to the is prior use in other experiments. Soaking the CNF causes the fibrils to become loose and flexible allowing for them to be pressed evenly against the surface of the crystal. Initial attempts to saturate the fibers used water, which resulted in complications due to the signature of water which obstructed all signs of the cellulose spectra due to the water peak found at 1643.5 cm^{-1}. (29) This peak directly conflicts with the cellulose peak of interest. When the fibrils were saturated to the point of compliance the peak became entirely covered. Ethanol was initially selected as a replacement media because of its spectra. Experiments with Ethanol to soak the fibrils found that Ethanol could not penetrate the fibril structure and they remained brittle preventing it from being useable as the media. A third medium Nujol was considered. Despite having a peak located around the area of interest both the peaks low intensity, as well as its ability to add compliance to the fibril system, made it the clear choice for use.(30)

Methods and materials

Particle Synthesis

Iron oxide nanoparticles are a highly useful group of particles due to their superparamagnetic nature. The properties of the particles are directly related to the size and dispersion of the colloidal system which in turn is depended on the synthesis method that is used to create it. Numerous methods exist for creating the Fe_2O_3 particles including but not limited to; precipitation reactions, high-temperature, decomposition of organometallic precursors, sol-gel reactions, and a multitude of others(19). For these experiments, a particle system with an average diameter of 9 nm and a dispersion media of water was chosen.(31) The size of the particles is critical as to allow the particles to easily fit into the cellulose system without congesting the pore structure of the fibrils. The decreased size adds additional protection against unprompted flocculation.

Using water as the dispersion media is similarly important as the cellulose is also dispersed in water. In addition, the particles being in water assists in the integration of the particles into biological systems as other solvents both organic and inorganic can cause problems in-vivo. To achieve the desired particle properties, a synthesis using both a co-precipitation reaction and thermal decomposition is required. These initial synthesis steps involve the co-precipitation of two iron salts: iron(II) chloride tetra hydrate and iron(III) chloride hexahydrate. Both salts are dissolved in 380ml of DI water and allowed to mix thoroughly at room temperature. Once the particles are evenly dispersed, 20ml of ammonium hydroxide is added dropwise. This process causes the salts to precipitate into Fe_30_4. The Fe_3O_4 particles are super paramagnetic but are too unstable to be used in this application. Once all the ammonium hydroxide is added the particles are separated by exploiting there newly formed paramagnetic properties. Once the particles have separated and have

been decanted from their solution, 60 ml of 2M nitric acid is added. Once the solution has been allowed to re-disperse 60 mL of iron (III) nitrate at 0.35M is added. The nitric acid allows for the ferric nitrate to better dissolve and promotes the oxidation of the Fe_3O_4. The particles are then placed over heat and refluxed for 1 hour, this step is critical as the surface layer of the particles need to oxidize to FE_2O_3 to increase their stability and usability. After reflux, the particles are made to sediment using a magnet and washed with both nitric acid and acetone. Each synthesis theoretically yields 2.18 gm of particles which are then re-suspended in 100mL of DI water. It is critical that the particle solution is not allowed to dry as after the acetone wash as this causes the particles to aggregate together and are difficult to completely re-suspend in solution. (31) Once the particles have been synthesis the particles need to be characterized to ensure the quality of the synthesis. Both UV-vis and DLS are used to quantitatively access the solution as well as qualitatively inspecting the solution against previous successful batches for color as well as the solutions susceptibility to a magnetic field.

Zeta-potential sweeps

Once it was determined that the native particle system was inadequately distributing on the cellulose fibers, the immediate solution was determined to be surface functionalization using a coating agent. Six different coating agents were selected; Tri-ethylene Glycol, Polyethylene Glycol 8000, Polyethylene glycol 20,000, Galactose, Xylose, and Dextran. In addition to testing multiple molecules as coating agents, multiple concentrations of each coating agent were tested. Ethylene glycol was chosen as it is an industry standard for the stabilization of colloidal systems on both extremes of the MW's. (32)(33) The ethylene glycol interacts with the surface of the particle via a physisorption and increases the

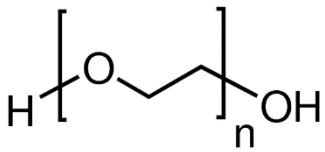

Figure 4 PEG Molecular Structure (image taken from public domain)

steric stability of the particles. In addition to increased steric stability of the particles, the PEG molecule has an abundance of sites for hydrogen bonding to the cellulose surface.(15) Figure 4 demonstrates the molecular structure of PEG. The intent is that while the particles are being mixed into the cellulose slurry the PEG will hydrogen bond the surface of the fibrils and cause the particles to uniformly disperse. To explore the effect that varying molecular weight has on both the colloidal system and the cellulose fibrils three different MW's were chosen spanning from TEG to the PEG 20,000. Due to the increased molecular weight of the PEG 20,000 and PEG 8000, the highest concentration of agent added was one order of magnitude lower than the initially purposed 0.01M.

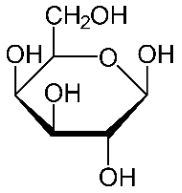

Figure 5 Galactose Molecular structure (image taken from public domain)

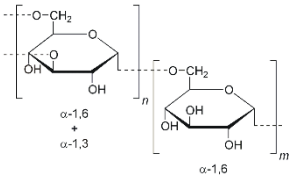

Figure 6 Dextran Molecular structure (image taken from public domain)

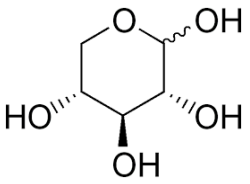

Figure 7 Xylose Molecular Structure (image taken from public domain)

The cellulosic sugars were selected for both their similarity to cellulose and the ability for the sugars to form hydrogen bonds. The three sugars chosen -- Galactose (figure 5), Dextran (figure 7), and Xylose (Figure 6) -- are all 5 carbon chains with alcohol functional groups like cellulose. The hydroxyl groups give all the sugars multiple sites for hydrogen bonding to both the cellulose and the Fe_2O_3 particles.(15) In addition, all the sugars listed have been previously demonstrated to stabilize colloidal systems. Dextran has been used for stabilization of Fe_2O_3 particles previously and for this reason, was selected as the first choice as the proposed stabilization agents.(34) (19) Xylose and galactose while not having been used to stabilize iron oxide particles have been used to stabilize other colloidal systems. (35) The molecular weight of the dextran solution caused similar limitations to the larger molecular weight polyethylene glycol and limited the concentrations of the dextran.

A stock solution for all the solutions were made at a concentration of 0.1M for all except PEG 8000, PEG 20,000, and Dextran which had initial concentration of 0.01M due to increased molecular weight. For each of the particle solutions prepared they were diluted to have a final optical density of 2, for both better measurements on UV-Vis and the DLS. Once the dilution of the particles is made 20 µL of 1M Nitric acid is added to prevent unnecessary fluctuation of pH. The particles are then allowed to mix thoroughly before the stabilizing agent is aliquoted into solution to achieve the final concentrations seen in Table 1. The solution is then allowed to mix for 24 hours to allow the particles to be thoroughly coated.

Table 1 Coating agent Concentrations for addition to Particles for pH Sweeps

No agent	**PEG 8000 (M)**	**PEG 20000 (M)**	**TEG (M)**	**Xylose (M)**	**Dextran (M)**	**Galactose (M)**
Stock	0.001	0.001	0.01	0.01	0.0001	0.01
	0.0001	0.0001	0.001	0.001	0.00001	0.001
			0.0001	0.0001		0.0001

After 24 hours, has elapsed, the particle solutions pH is measured and recorded. The solutions pH is then brought down to 2.5 using 1 M nitric acid. For future analysis, 1 mL of the particle solution is the reserved in a cuvette. In addition, a sample is collected and reserved for zeta-potential analysis. Using 0.25M NaOH, the solution is brought up by pH increments of 0.5. As well as taking a sample and finding the zeta-potential at each increment record the volume of NaOH aliquoted to cause the increase in pH is recorded. A final quantitative measure, when the solution became visually cloudy the pH was recorded. Once the solution reaches a pH of 11.5, the final solution is collected and the UV-Vis spectra is recorded for each sample and size the particles at

both the 2.5 pH point and the flocculation pH. This procedure allows for the identification of coating agents that grant increased pH stability as well as the ability to observe any interesting interaction that will be caused by the addition of the coating agent.

Once all the particle solutions have gone through the pH sweep eight conditions are selected, these solutions were selected to explore the highest variety of solutions possible, PEG 8000 is omitted due to its results being similar to the PEG 20,000 and a more in-depth exploration of Dextran's behaviors shown in results and Discussion (pages 24-25) addition for reasoning. Each of these eight conditions are mixed into cellulose by preparing a solution totaling 20 mL (Table 2).

Table 2 Final Coating solution for Integration into Cellulose Fibrils

	Volume particles (2/2/17 synthesis batch)	**Volume coating agent**	**Volume DI water**
Positive Control	0.800 mL	0 mL	19.2 mL
Dextran 0.0001M	0.800 mL	2.00 mL (0.001M Dextran)	17.2 mL
Dextran 0.00001M	0.800 mL	0.200 mL (0.001M Dextran)	19.0 mL
TEG 0.01M	0.800 mL	2.00 mL (0.1 M TEG)	17.2 mL
Galactose 0.001M	0.800 mL	0.200 mL (0.1 M Galactose)	19 mL
Xylose 0.001M	0.800 mL	0.200 mL (0.1 M Xylose)	19 mL
PEG 20,000 0.001M	0.800 mL	2.00 mL (0.01 M PEG 20,000)	17.2 mL
Negative Control	0 mL	N/A	20 mL

Once all the solutions have been prepared, a 10 mL aliquot is taken and combined with 10 mL of CNF slurry. The solution is mixed both through agitation of solution and sonication to ensure the solution is homogenous. Each solution is then divided equally into two gem boxes. The boxes are then placed with the lid open into the oven, set at 45 C, for 72 hours.

Results

UV-Vis data

While preforming the pH sweeps of all particle systems, the key behavior of interest is the flocculation of the particles. As described previously the particles in their non-flocculated state have a UV-Vis absorbance peak around 450 nm. Once the particles have become destabilized this peak broadens and shifts rightward. This trend is clearly seen in Figure 8 where the initial curve of the solution collected at pH 2.38 has peak of 450 nm with a bandwidth of 91 nm. When the particles flocculate the absorbance peak shifts right to 530 nm and the bandwidth increase to 476 nm.

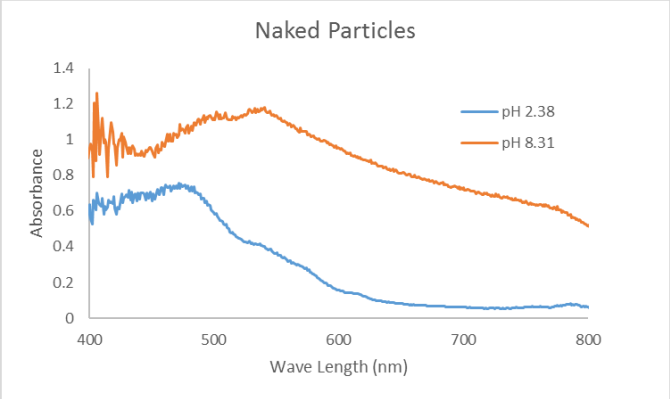

Figure 2 Naked Particles UV-Vis Spectra During pH Sweep

The key goal of this research is to develop methods to prevent the particles from flocculating to make them easier to integrate into the cellulose. Therefore, during the pH sweep, the particles were monitored for aggregation both before and after the pH sweeps. In addition to watching for flocculation, the pH of flocculation is recorded. Due to the innate noise of the system, all peaks and bandwidths are approximate, to account for this measurement error, the UV-Vis data 5 points are average.

While testing the three variations of polyethylene glycol at multiple concentrations, three cases one of each type, has been selected to exemplify the trend seen in all other cases for that stabilization agent. Figure 9 is indicative of the effect that the addition of TEG had to the particle system in terms of prevention of aggregation; that is, little to none. The initial peak can be found

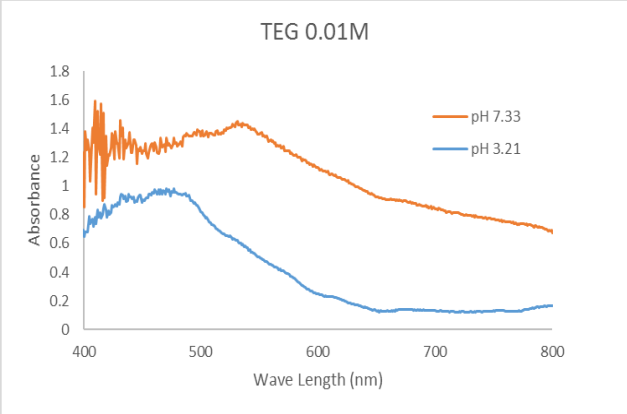

Figure 8 TEG 0.01M UV-Vis Spectra During pH Sweep

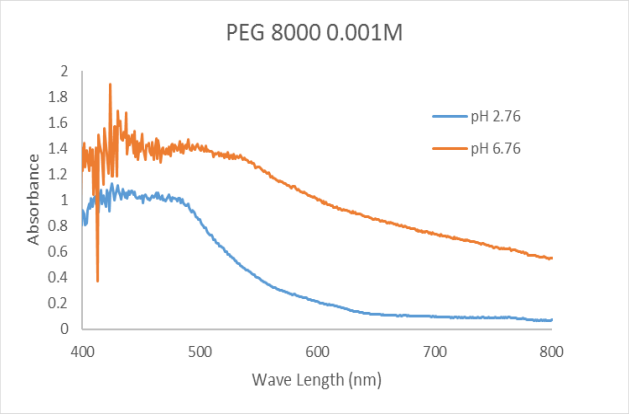

Figure 9 PEG 8000 0.001M UV-Vis Spectra During pH Sweep

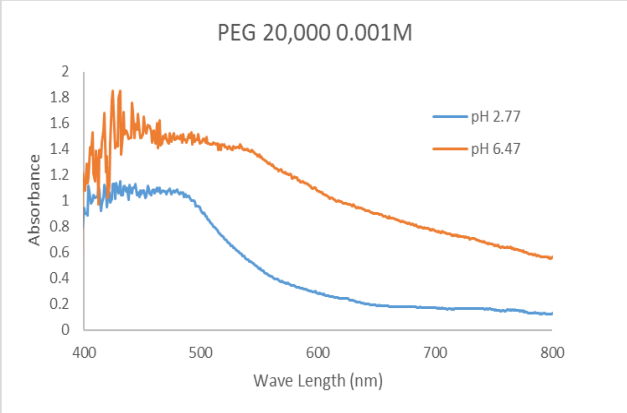

Figure 10 PEG 20,000 0.001M UV-Vis Spectra During pH Sweep

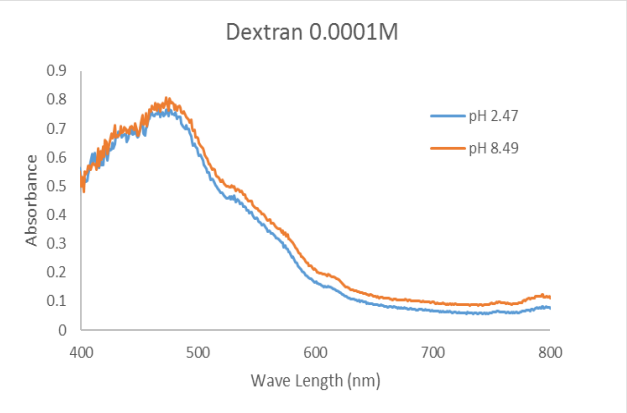

Figure 11 Dextran 0.0001M UV-Vis Spectra During pH Sweep

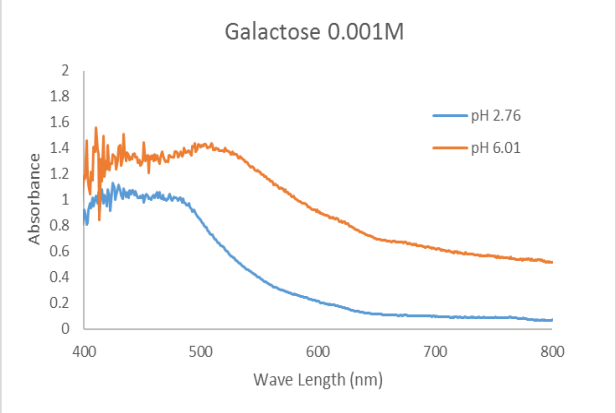

Figure 12 Galactose 0.001M UV-Vis Spectra During pH Sweep

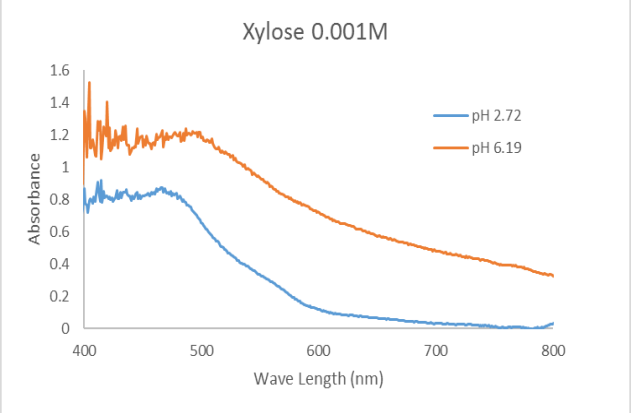

Figure 13 Xylose 0.001M UV-Vis Spectra During pH Sweep

at 455 nm, and the bandwidth of 188. Once the particles reach pH 7.33 they flocculate and have band width of 464 nm and a peak of 532 nm. Figure 10 is an indicator of the PEG 8000. The initial peak can be found at 450 nm and a bandwidth of 162. Once the particles reach a pH of 6.76 the particles flocculated and the peak shifts to 488 nm and the bandwidth to 414 nm. Figure 11 is a representation of the PEG 20,000 results. The initial peak can be found at 454 nm and the bandwidth is 182 nm. When the pH reaches 6.47 the peak of 484 nm and the bandwidth increases to 446 nm.

The cellulosic sugars are compared similarly, three of the experiments have been selected which illustrate the trends observed in the experiments preformed on each of the coating agents. Dextran at 0.0001M has an initial peak at 466 nm and a band width of 162 nm. Throughout the entirety of the pH sweep this remains constant a section at pH 8.49, past the point of flocculation for other particle systems, has been selected. At the pH of 8.49, the peak can be found at 472 nm and the bandwidth is 168 nm. This is the only coating agent that had any pronounced effect on the particles stability in solution. Particles remained not only from the perspective of the UV-Vis but as later will be shown the DLS. Galactose 0.001M, represented in figure 13, has an initial peak at 461 nm and a bandwidth of 170 nm. At pH 6.01 the peak increases to 498 nm and the bandwidth increases to 300 nm. Xylose the final coating agent tested has an initial peak at 465 and a band width of 128 nm. The peak after flocculation at pH 6.19 has a peak at 508 nm and a bandwidth of 266 nm.

The UV-Vis results show that all the particle system resisted flocculation during the coating process, supported by the peak structure of all coating agents before the sweep. This makes all system eligible for integration onto the cellulose fibrils in later experiments. Only the Dextran granted any makeable increase the particles ability to resist pH changes.

Zeta Potential Results

As the pH of the solution, the particle solution in slowly increased from the native 2.5 the zeta potential goes from a positive to negative. At values, above or below 25mV/-25mV the particles are highly stable. As the electrical potential approaches 0mV, the electrostatic stabilization is overwhelmed and the particles flocculate.(36) These near 0mV values is where the particle system had been experiencing flocculation. To ensure the validity of the pH sweeps preformed the zeta potential curve for all sweeps was collected (Figure 15-20). As seen in the Zeta Potential Curves Collected all particle system behaved in the same way, a sigmoidal relationship as the pH increases. For the TEG, PEG 8000, Galactose and Xylose zeta potential curves they all start and finish with approximately the same value 50mv and -50 mV. This is in keeping with the bare particle system (Figure 1). The similarity in curve value points to the coating agent not interfering with charge surface of the particles and simply binding to it. Both the PEG 20,000 and Dextran observed a different start and finish zeta potential value much lower than the initial. (Figures 17 and 18) In these cases, the Zeta potential starts in a region that classically would be considered a instable area for colloidal systems, being between 25 mV and -25 mV. Despite this, both are stable in solution as shown by the UV-Vis spectra (Figures 11 and 12).

Zeta potential curves (figures 15-20)

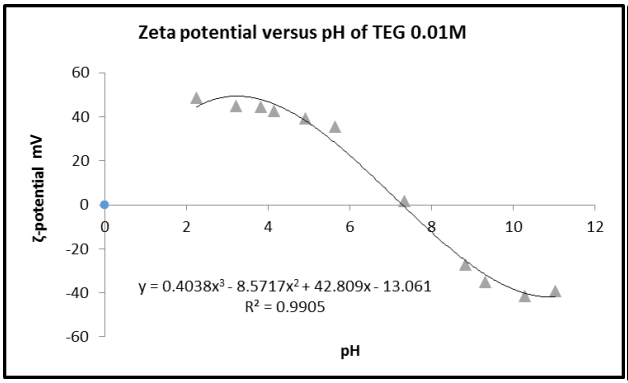

Figure 14 TEG 0.001M Zeta Curve

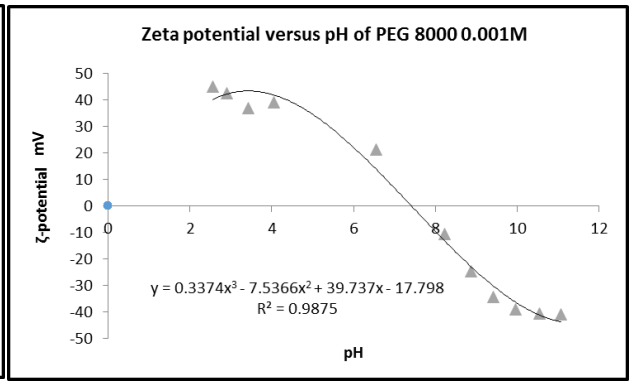

Figure 15 PEG 8000 0.001M Zeta Curve

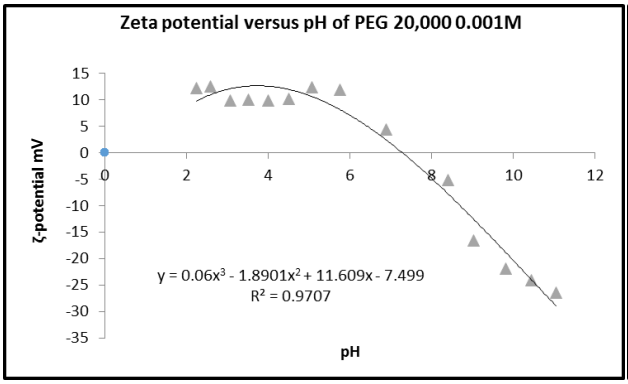

Figure 16 PEG 20,000 0.001M Zeta Curve

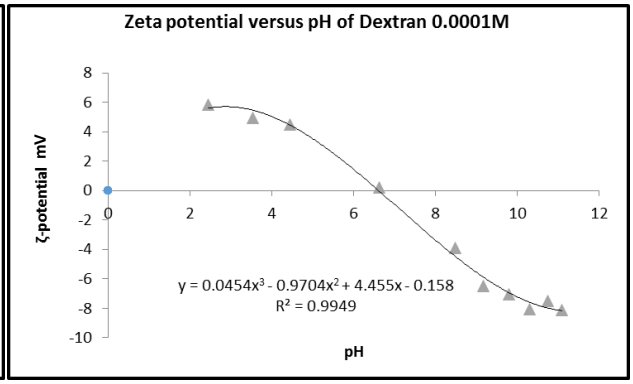

Figure 17 Dextran 0.0001M Zeta Curve

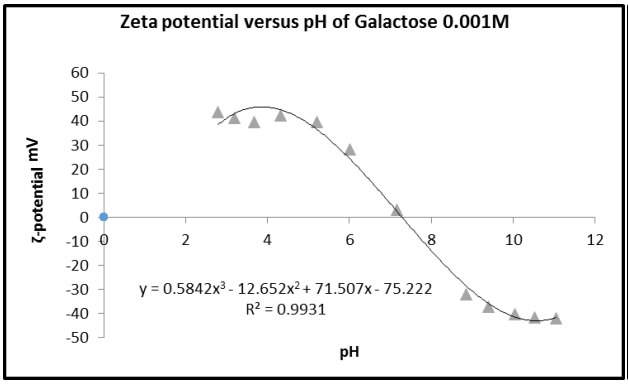

Figure 18 Galactose 0.001M Zeta Curve

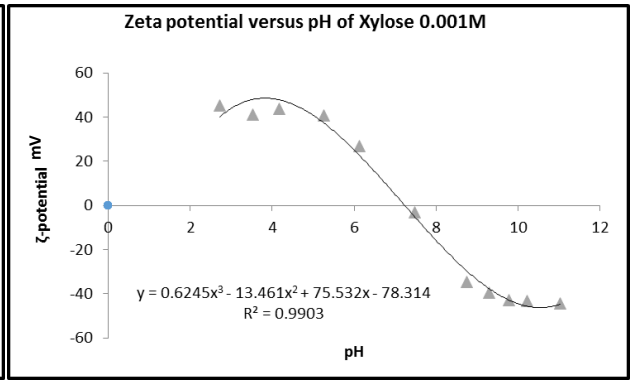

Figure 19 Xylose 0.001M Zeta Curve

DLS results

The initial function of the DLS is to characterize the particles from the reactor to ensure the quality of the synthesis: the particles should have a monodisperse peak at or around 10-20 nm and no flocculation should have occurred. Figure 21 is the characterization of one particle batch which shows the graph of a useable particle batch. The large peak found at the right end of the distribution are aggregates that are a byproduct of the synthesis and are a small enough proportion that they do not affect the overall quality of the batch. It is also observed that the particles post synthesis cannot be allowed to dry post Acetone wash or the particles. This causes the particles to aggregate together and all attempts to separate via intense sonication particles failed, this is seen in the Figure 23. Once the particles have been characterized, the function of the DLS shifted to measure the effect that the coating agents had on the colloidal system as well as monitoring the system during the pH sweeps. For all the coating agents, the DLS demonstrated the same trend of the UV-Vis the particles post synthesis, the results were consistent throughout all experiments and will be demonstrate in the PEG 20,000 0.001M. Post addition of coating agent the particles experience as slight rightward shift with the peak moving from 23 nm in the synthesis DLS measurement to 34 nm (Figure 22). This increase in size is caused by the addition of the polymer to the surface of the particle, this does not seem to be an indication of flocculation supported by both the UV-Vis data (Figure 11) where the peak can still be found at 454 nm as opposed to the rightward shift expected in aggregation. In addition, the increase in size is less than double that of the physical particle this doubling in diameter is the minimum size increase for flocculation behavior. The particle systems also behaved similarly when the particles reached the flocculation pH the particles experienced a dramatic rightward shift with the average size of particles being above 2000 nm (Figure 24), this is consistent with UV-Vis data and is indicative of aggregation.

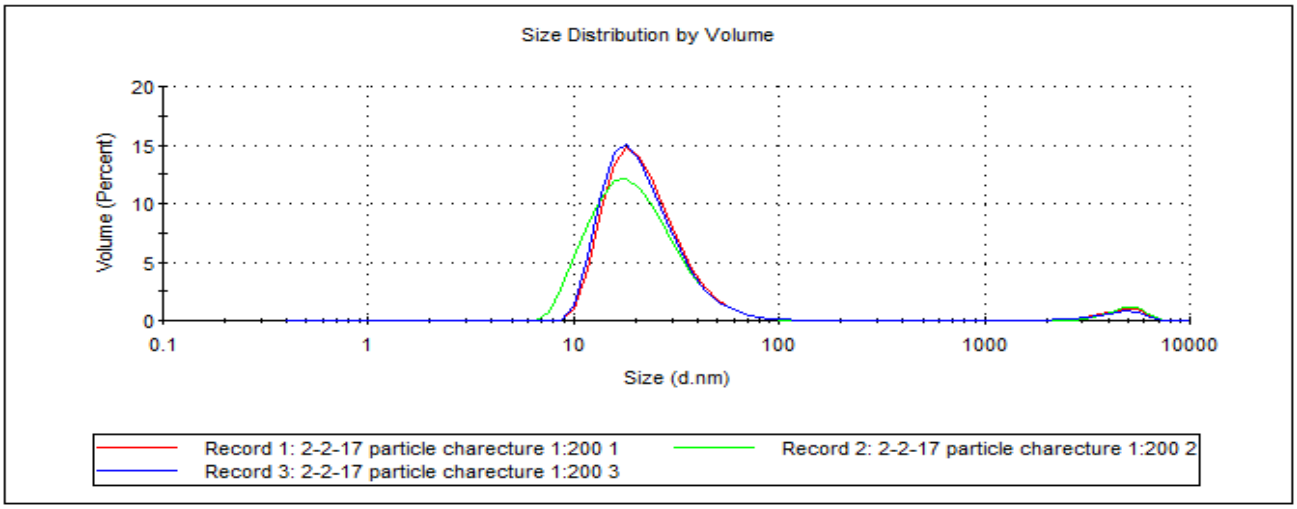

Figure 20 Naked Particles Characterization

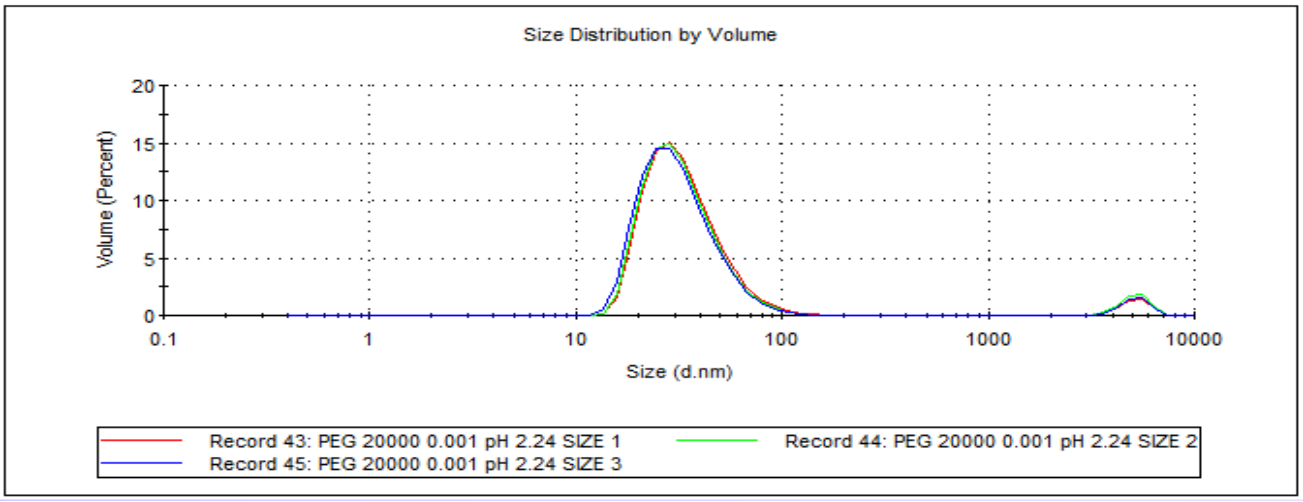

Figure 21 PEG 20,000 0.001M DLS pH 2.24

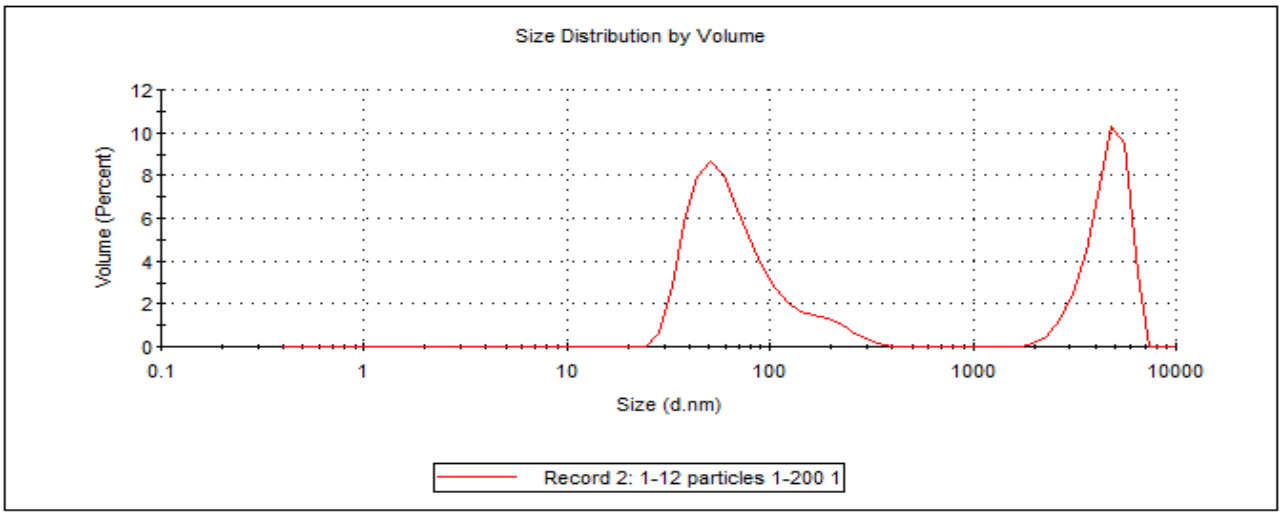

Figure 22 Air Dry Particle Synthesis

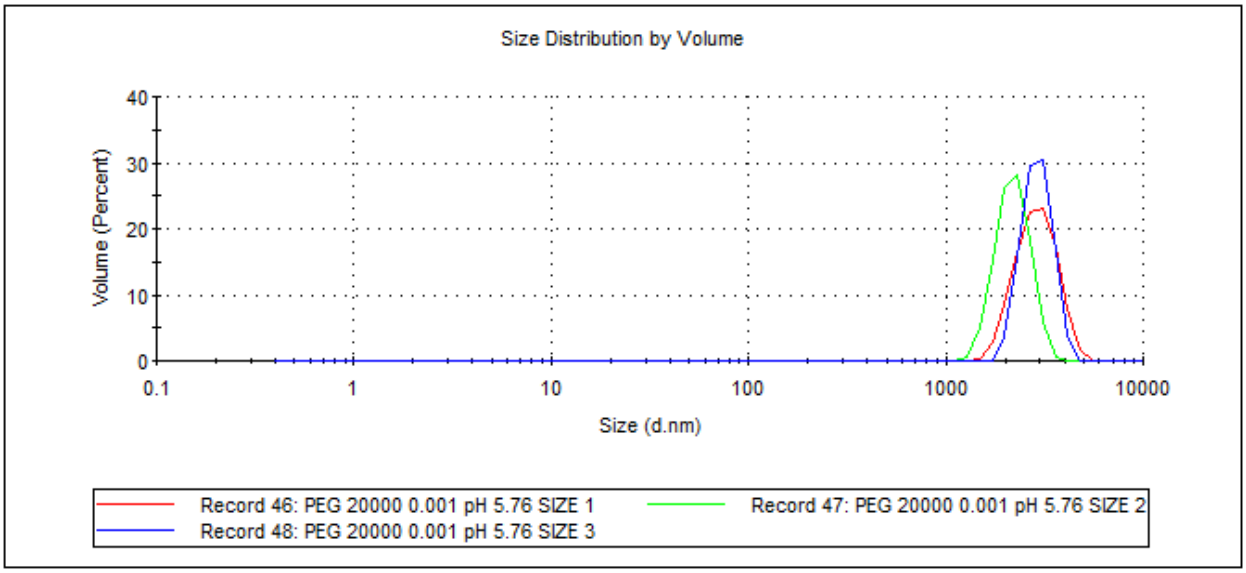

Figure 23 PEG 20,000 0.001M pH 5.76

SEM Results

The SEM is used as a qualitative analysis of the coverage of the particles on the fibrils. Due to the nature of both the particles being super paramagnetic they needed to be sputter coated in gold/palladium to allow the samples to be visually inspected by the SEM. In addition, the coating agent visual distortions to the image are caused both by heat of the SEM which causes cracking in the surface fibrils and image blurring caused by the uneven surface of the amalgam. The Figure 25 demonstrates the fibrils without any particles added. It is observed that the individual fibrils are clearly visible and are distinct from each

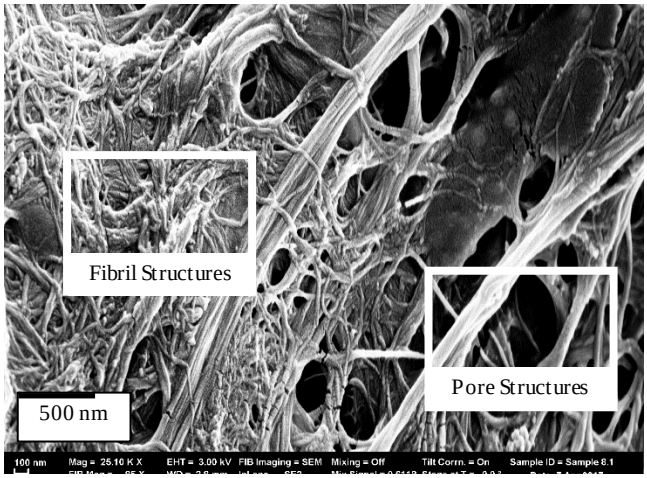

Figure 24 SEM Bare Fibrils (25K X)

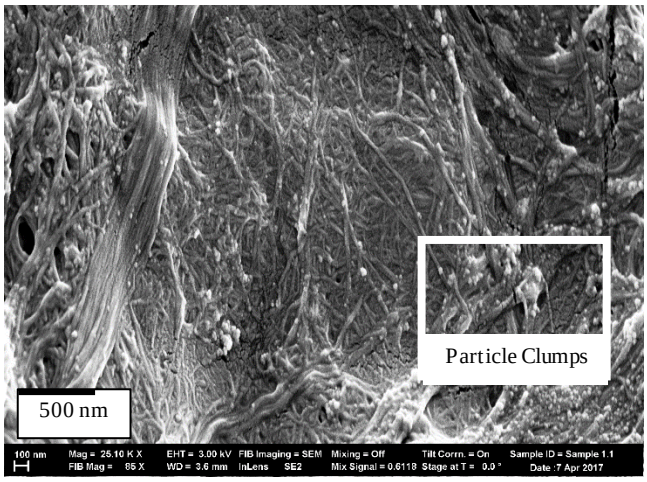

Figure 25 SEM Naked Particles (25K X)

of the other fibrils. The porous structure of the cellulose is also clearly visible; in the ideal coating method, these pores will remain viable as they are critical for osteocyte integration. Figure 26 is representative of the naked particles being added to the surface of the fibrils; there are clear areas of dense particle (lower left hand corner) as well as clumps of particles, small rounded clumps dispersed through the fibril matrix. In addition, there areas where the individual fibrils without any coverage of particles, assessed by the roughness of the area, seem to still be visible. Reducing these inconstancies in particle coverage is the primary goal of this experiment. The individual pores of the fibril structure can still be seen (left hand side middle) but are decreased in number, it is unknown if that is a function of the particle coating of the location that the image was taken. Figure 27, Dextran 0.0001M, has decreased quantities of the particle clumps and appear to be more evenly dispersed throughout the entire fibril as opposed to being clumped in sections. The lines between the induvial fibrils appear less defined suggesting that the fibrils are less defined due to the coating of particles smoothing the general structure. The individual pore structures remain visible but appear more rounded. Dextran at 0.00001M, Figure 28, has a more diminished

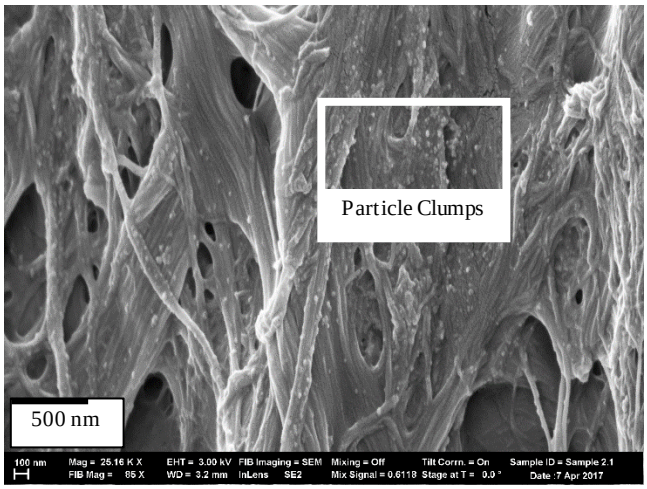

Figure 26 SEM Dextran 0.0001M (25K X)

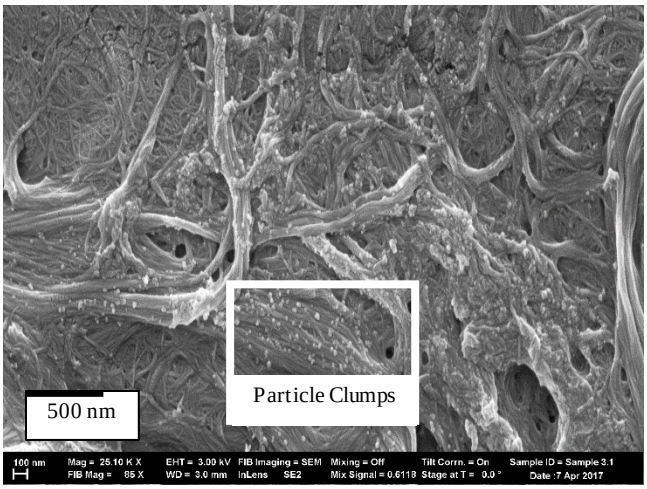

Figure 27 SEM Dextran 0.00001M (25K X)

smoothed appearance when compared to of the dextran 0.0001M. In addition, there appears to be a less even distribution of the particle clumps. In addition to a less even distribution the particles clumps appear more numerous suggesting a less though distribution of the particles across all fibrils. TEG 0.0001M, Figure 29, the particle clumps are increasingly numerous and unevenly distributed. The clumps have become so concentrated that in areas the particles have taken on a cauliflower like appearance while the contracts of individual fibrils are like the Dextran 0.00001M suggesting a decreased even coverage. The galactose 0.001M, Figure 30, has a further increased cauliflower appearance with large clumps of particles covering most of the entire surface. The particles have clumped together in large sections while there are clear areas where the particles have not attached to fibril sections as the induvial fibrils remain as visible as when no particle system were added. Xylose

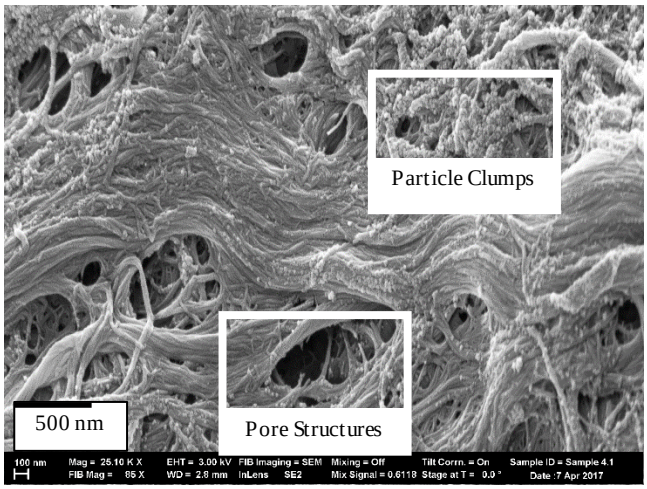

Figure 28 SEM TEG 0.01M (25K X)

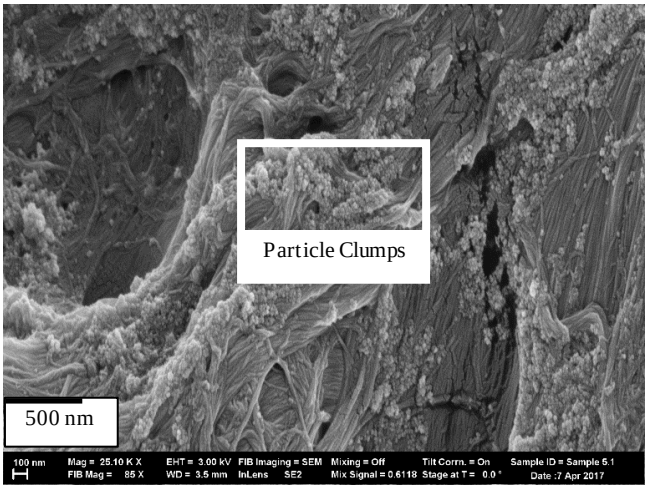

Figure 29 SEM Galactose 0.001M (25K X)

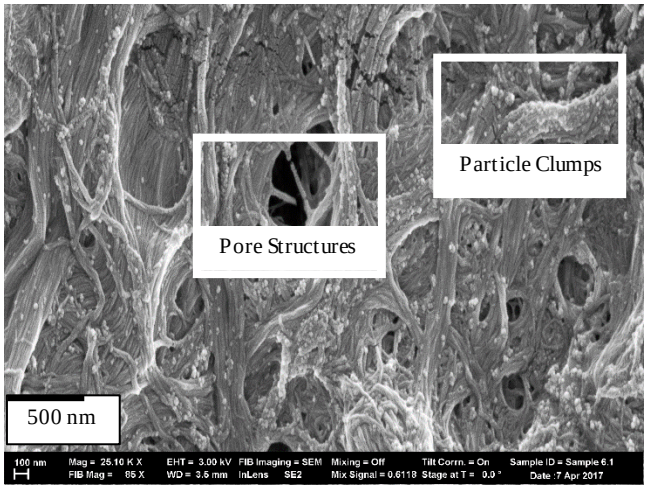

Figure 30 SEM Xylose 0.001M (25K X)

0.001M, Figure 31, the particle clumps not in the large sections that is observed in TEG 0.01M, Figure 29 and galactose 0.001M, Figure 30, but are more evenly dispersed. The Overall quantity of the particle clumps remain high signifying inadequate integration. The contrast between individual fibrils is high. The PEG 20,000 0.001M is the most unique of all the matrixes. The coating has taken on an entirely smooth surface. The Peg 20,000 on the fibrils has given a sticky, "syrup-like" appearance and the particles (the glowing dots within the coating) are evenly dispensed. The PEG 20,000 0.001M samples also maintained some of the native pore structure although it is highly probable that due to the apparent viscosity of the coating agent that some pores are covered. In addition to the differences illumined by the SEM the PEG 20,000 in the cellulose had other visual differences. For all other Cellulose samples with or with coating agent as the system dries the fibrils bend and buckle creating a distorted final product (figure 33A). For the PEG 20,000 the cellulose dried entirely flat (Figure 33B). This unexpected result is most likely due to the PEG 20,000 reducing the available hydrogen binding sites between the fibrils. This Phenomena needs to be explored further before any true discussion can be had.

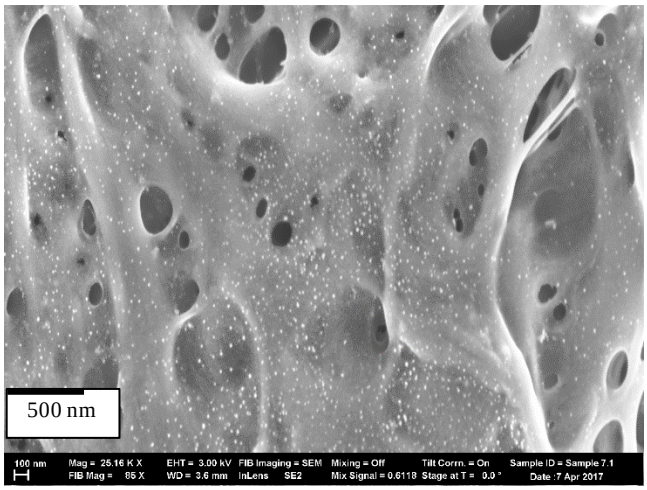

Figure 31 SEM PEG 20,000 0.001M (25K X)

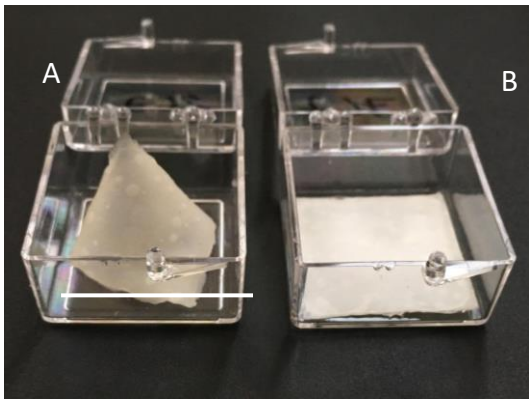

Figure 32 No coating agent (A) PEG 20,000 (B) Air Dried Cellulose Fibrils

FTIR Results

The purpose the FTIR is to quantitatively analysis the coverage of the iron oxide Nano-Particles with their coating agent onto the fibrils. The methodology used the bare cellulose FTIR signature was compared to the FTIR signature of all seven conditions for coating agents. The Primary area of interest is the cellulose aromatic peaks found at 1542 cm^{-1} and 1506 cm^{-1}. (37) A reduction in these peaks suggests that the cellulose fibrils have become sufficiently covered in the iron particle

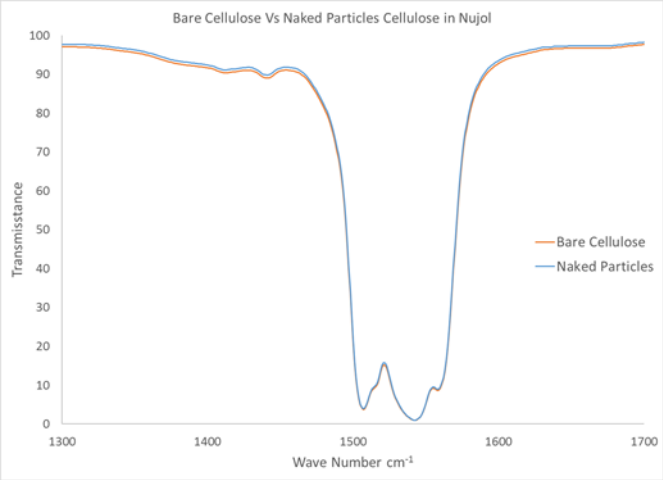

Figure 33 Bare Cellulose vs Naked Particles FTIR (1300-1700) cm-1

Percent Reduction Transmittance		
Wave Number	1542 cm-1	1506 cm-1
Bare	-0.38	-0.38
Dex 0.0001 M	9.32	16.50
Dex 0.00001 M	9.71	19.06
TEG 0.001M	6.19	5.98
Galactose 0.001M	6.80	6.73
Xylose 0.001M	6.64	6.41
PEG 20,0000 0.001M	21.0	27.0

Table 3 FTIR 1300-1700 cm-1 Percent Decrease Transmittance from Bare Cellulose

system that the signature has come disguised. For each spectra, the peak value transmittance is standardized by using the transmittance found at 1682 cm^{-1} and is then compared to the bare cellulose peak by Percent reduction in the transmittance, these values are shown on Table 3. The

Bare particles, figure 34, are shown to not affect the cellulose aromatic peak, having a -0.38% reduction in transmittance, this is consistent with the previously observed behavior of the particles not completely binding to the surface. The Dextran solutions, Figures 35 and 36, saw a dramatic percent decrease in transmittance intensity as compared to the bare cellulose. The Dextran 0.0001M had a 9.32% decrease in the 1542 cm^{-1} and a 16.50% in the 1506 cm^{-1} peak. The dextran 0.00001M saw an increased drop in transmittance 9.71% in the 1542 cm^{-1} and a 19.06% decrease in the 1506 cm^{-1} peak. These results are consistent with the SEM data in which the most pronounced smooth coverage and even distribution were resultant of the dextran samples. The remaining samples, Figures 37- 39, apart from PEG 20,000 saw near identical reductions in the peaks 6.5% ± 0.4% in the 1542 cm^{-1} and a 6.40% ± 0.4% in the 1506 cm^{-1} peak. These results are similarly consistent with the SEM images where the visually similar in coverage and particle distribution. The PEG 20,000 0.001M, Figure 40, saw a 21.0% in the 1542 cm^{-1} and a 27.0% in the 1506 cm^{-1} peak. This decrease in the transmittance intensity is expected when the SEM images are viewed as the entire surface of the fibrils appear to be covered in the PEG 20,000 solution. In addition, the radically increased mass of the PEG 20,000 coupled with the high concentration of material lead to a much larger amount of material being added to the fibrils which most likely had a profound effect on the surface characteristics.

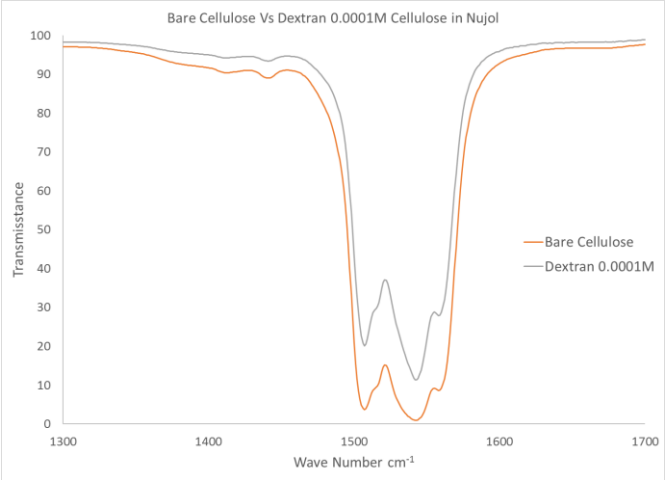

Figure 34 Bare Cellulose vs Dextran 0.0001M FTIR (1300-1700) cm-1

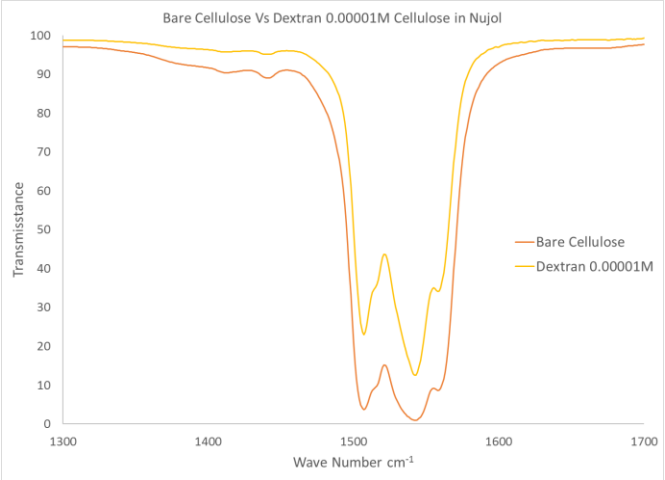

Figure 35 Bare Cellulose vs Dextran 0.00001M FTIR (1300-1700) cm-1

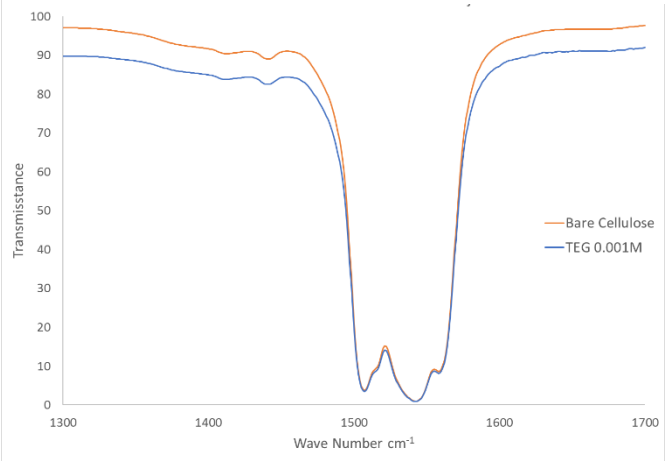

Figure 36 Bare Cellulose vs TEG 0.01M FTIR (1300-1700) cm-1

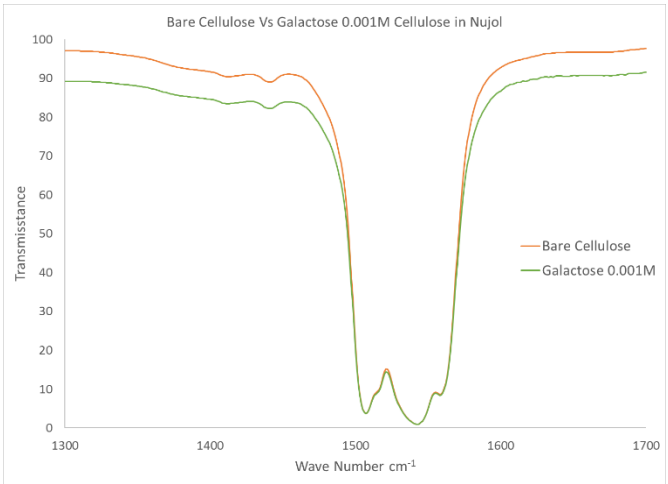

Figure 37 Bare Cellulose vs Galactose 0.001M FTIR (1300-1700) cm-1

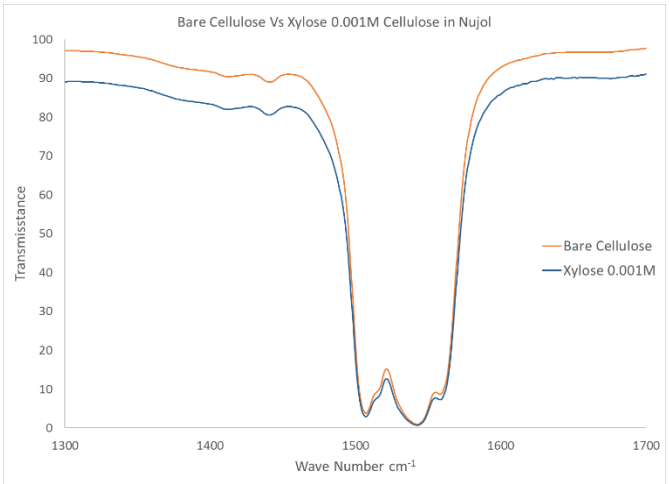

Figure 38 Bare Cellulose vs Xylose 0.001M FTIR (1300-1700) cm-1

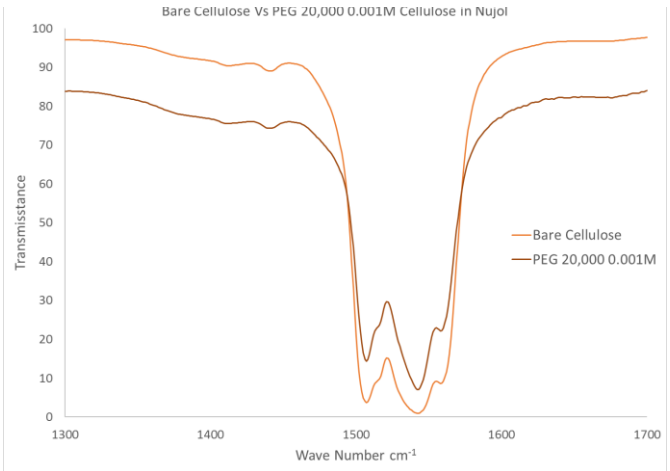

Figure 39 Bare Cellulose PEG 20,000 0.001M FTIR (1300-1700) cm-1

An addition rejoins of interest in the IR spectra collected is found in two peaks located between 1150 cm^{-1} and 1400 cm^{-1}. These peaks correlate to hydroxyl functional groups (37), the anticipated result for the hydroxyl groups peak was a reduction due to the particles covering the surface of the cellulose which figure 3 shows is a key part of its structure. All the systems demonstrated an increase on the peak intensity at 1300 cm^{-1} as seen in table 4. After consideration, it became clear that the reason for the decrease in transmittance is due to the structure of the coating agents used. As seen in Figures 4-6 the coating agents used all have hydroxyl groups. This physical characteristic of the coating agents makes the decreased transmittance both an expected result and a useful tool to explore the success of the coating agent's addition to the surface. These trends can

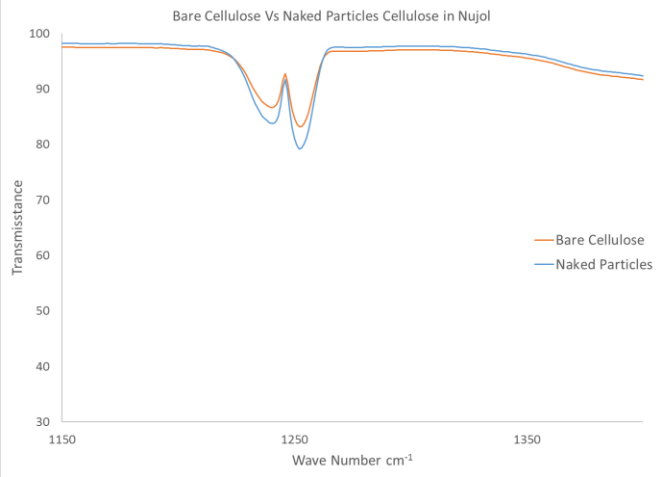

Figure 40 Bare Cellulose vs Naked Particles FTIR (1150-14000) cm-1

be seen in Figures 44-46. The naked particles addition to the cellulose say the smallest decrease in transmittance, Figure 41. The decrease in transmittance associated with the addition of the naked is most likely due to either the surface layer of oxygen (19) on the particles having bonded with free hydrogen ions forming a hydroxide group or addition confounding effects that need further exploration. The Dextran solutions, figures 42 and 43 have the next smallest decrease in transmittance. This is in keeping with the structure of the dextran polymer which has a low number of hydroxyl groups when compared to the remaining cellulosic coating agents. The remaining all

had further decreased peak intensities which correspond to the increased number of hydroxyl groups found on both the Galactose, Xylose and the Ethylene glycol polymers. Due to these confounding effects of the coating agent it is difficult to quantitatively say if the success coating agent's addition to the fibrils can be directly correlated with the decrease in transmittance.

Percent Reduction Transmittance from cellulose	
Wave Number	1300 cm^{-1}
Bare	-33.74
Dex 0.0001 M	-54.09
Dex 0.00001 M	-129.11
TEG 0.001M	-153.80
Galactose 0.001M	-169.37
Xylose 0.001M	-174.29
PEG 20,000 0.001M	-209.63

Table 4 Percent Reduction Transmittance from Cellulose FTIR 1300 cm-1 hydroxyl peak

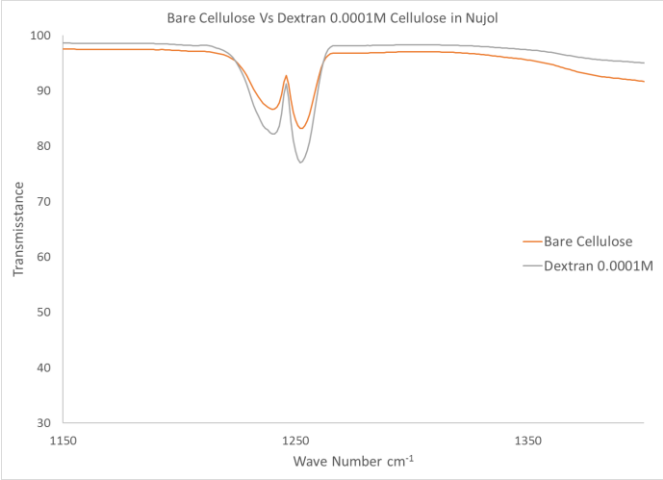

Figure 41 Bare Cellulose vs Dextran 0.0001M FTIR (1150-1400) cm-1

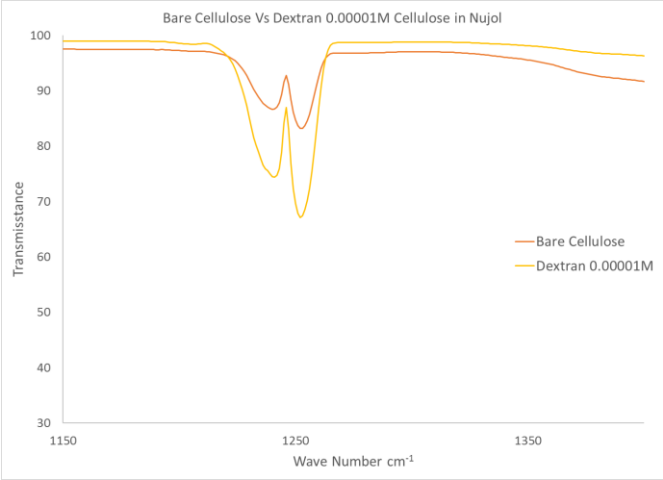

Figure 42 Bare Cellulose Vs Dextran 0.00001M FTIR (1150-1400) cm-1

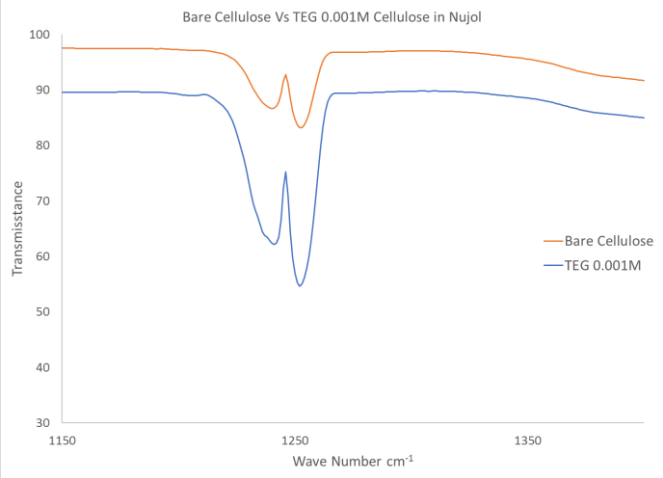

Figure 43 Bare Cellulose vs TEG 0.01M FTIR (1150-1400) cm-1

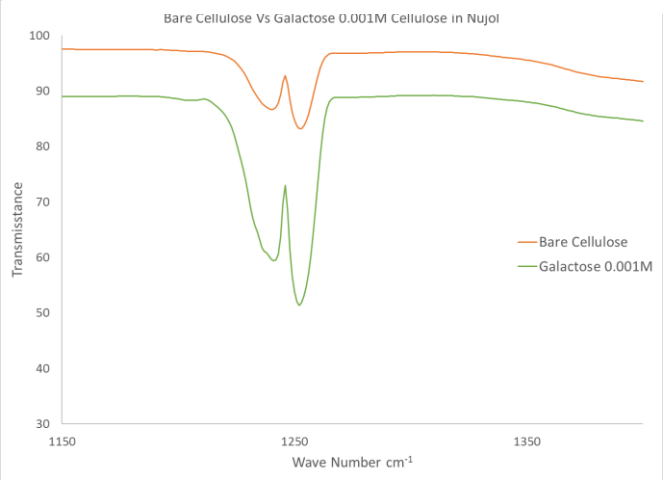

Figure 44 Bare Cellulose vs Galactose 0.001M FTIR (1150-1400) cm-1

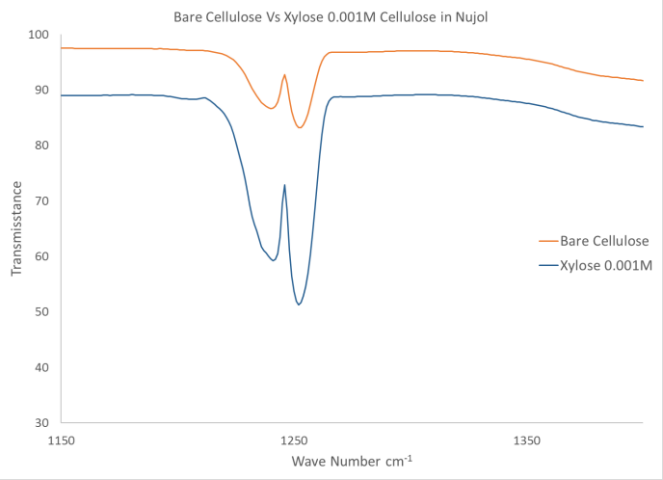

Figure 45 Bare Cellulose vs Xylose 0.001M FTIR (1150-1400) cm-1

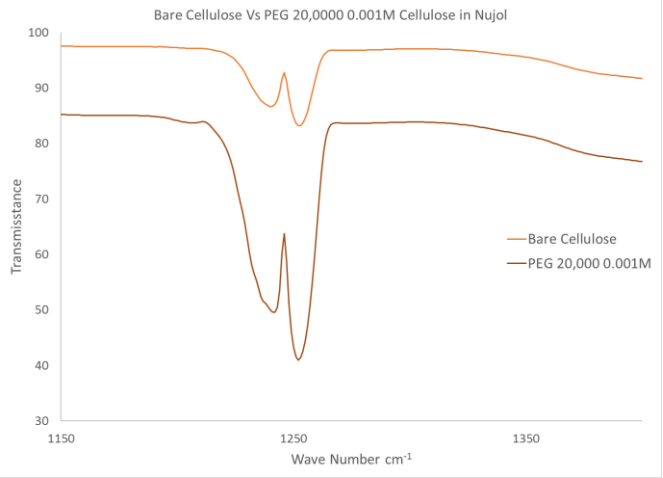

Figure 46 Bare Cellulose vs PEG 20,000 0.001M FTIR (1150-1400) cm-1

A final experiment conducted is a preliminary venture into the effect that coating agents have on the drying process. Four separate molecular weights of PEG were chosen and a total of nine different conditions were created with varying Peg MW and molarities. The samples were integrated with the same procedure as the integration of the coated particles systems. The cellulose samples were then qualitatively examined for flatness and compared to the ration of mass PEG integrated into the system and Mass of cellulose. Primary results point to the higher the ratio of the PEG to cellulose causes a more pronounced flattening effect.

PEG MW	1000	1000	6000	6000	8000	8000	8000	20000	20000
Molarity	0.001	0.0001	0.001	0.0001	0.01	0.001	0.0001	0.001	0.0001
MASS PEG: Mass Cellulose	0.0007	0.0001	0.004	0.0004	0.0533	0.0053	0.0005	0.0013	0.0133

Table 5 Variable PEG MW and Molarity for testing of drying phenomena

Discussion

The results for particle systems pre-integration into the cellulose indicate that the addition of the coating agents affects the flocculation of the particles and maintain their viability. This property has the potential of being exploited in the future by both using the dextran agent to resist flocculation and further exploration to find addition coating agents that grant other properties to the particles. This would allow the particles to be highly tunable in function; either by being used to cause flocculation in certain circumstances or controlled releases of particles under certain stimuli. The variability in the particle addition behavior to the fibrils with the variable coating agent also points to the possibility of controlled release being a possibility after future experiments. The coating agents effect on drying behavior, as well as possible bulk material, needs to also be explored as it could allow for a wider variety of uses for the material.

Conclusions

Here we have shown that Iron oxide Nano particles can be successfully coating in various media, the coating agents can affect the flocculation behavior of the particles, the coating agents influence both the particles ability to coat cellulose nanofibrils as well as the cellulose Nano fibrils drying behavior. The ability for the particles to be coated in various materials both standard polymeric structures and cellulosic sugar both in monomeric and polymeric forms indicates the ability for these particles to be in the future functionalized with various coating agents to achieve specific behaviors. For integration into the cellulose nanofibrils, the use of dextran as a coating agent allows for a more homogenous distribution of the particles across the surface of the fibrils as well as more complete coverage of the surface of the fibrils. In addition, the ability to modify the drying characteristics of the cellulose will allow for future exploration into potential uses for the material. The use of these methodologies will allow for better integration of the particles into the cellulose nanofibrils and will grant the cellulose the ability to be imaged by both X-ray and MRI technologies for future use in medical implants.

Bibliography

1. Potulski DC, De Muniz GIB, Klock U, De Andrade AS. Green Composites from Sustainable Cellulose nanofibrils: A reveiw. Sci For Sci [Internet]. 2014;40(103):345–51. Available from: http://dx.doi.org/10.1016/j.carbpol.2011.08.078
2. Carter N. Physical Properties of Iron Oxide Nanoparticles. 2015;
3. Long M, Rack HJ. Titanium alloys in total joint replacement--a materials science perspective. Biomaterials. 1998;19(18):1621–39.
4. Kemp HBS, Sneath RS, Walker PS. Custom-Made Prosthetic Replacements for Bone Tumours of the Lower Limb. Bone Joint J. 1996;78–B(1):5–13.
5. Banaszkiewicz PA. Porous-coated hip replacement. The factors governing bone ingrowth, stress shielding, and clinical results. Class Pap Orthop. 2014;69(1):51–5.
6. Tronzo RG. Bone implant with Porous Exterior Surface. 1997;10–3.
7. Stephenson PK, Freeman M a, Revell P a, Germain J, Tuke M, Pirie CJ. The effect of hydroxyapatite coating on ingrowth of bone into cavities in an implant. J Arthroplasty [Internet]. 1991;6(1):51–8. Available from: http://www.ncbi.nlm.nih.gov/pubmed/1849985
8. Turvey TA, Bell RB, Tejera TJ, Proffit WR. The use of self-reinforced biodegradable bone plates and screws in orthognathic surgery. J Oral Maxillofac Surg. 2002;60(1):59–65.
9. Jones DA, Lucas HK, O'Driscoll M, Price CHG, Wibberley B. Cobalt toxicity after mckee hip arthroplasty. J Bone Joint Surg Br. 1975;57–B(3):289–96.
10. Staiger MP, Pietak AM, Huadmai J, Dias G. Magnesium and its alloys as orthopedic biomaterials: A review. Biomaterials. 2006;27(9):1728–34.
11. S B. Effects of Recumbency on. Bone. 1967;1194–205.
12. Carlsson CA, Carlsson GA. Basic physics of X-ray imaging. Linkoping Univ. 1996;3–29.
13. Hadjizadeh A, Doillon CJ. Directional migration of endothelial cells towards angiogenesis using polymer fibres in a 3D co-culture system. J Tissue Eng Regen Med. 2010;4(7):524–31.
14. Helenius G, Bäckdahl H, Bodin A, Nannmark U, Gatenholm P, Risberg B. In vivo biocompatibility of bacterial cellulose. J Biomed Mater Res - Part A. 2006;76(2):431–8.
15. Siro I, Plackett D. Microfibrillated cellulose and new nanocomposite materials: A review. Cellulose. 2010;17(3):459–94.
16. Palmqvist AEC. Synthesis of ordered mesoporous materials using surfactant liquid crystals or micellar solutions. Curr Opin Colloid Interface Sci. 2003;8:145–55.
17. Mason M, Holomakoff D, Hossen M. Controlled Porosity Strucutral Material with NanoCellulose Fibers. Orono, ME: University of Maine Patent Office; 2015.
18. Weishaupt D, Kochli VD, Marincek B, Kim EE. How Does MRI Work? An Introduction

to the Physics and Function of Magnetic Resonance Imaging. Vol. 48, Journal of Nuclear Medicine. 2007. 1910-1910 p.

19. Laurent S, Forge D, Port M, Roch A, Robic C, Vander Elst L, et al. Magnetic iron oxide nanoparticles: Synthesis, stabilization, vectorization, physicochemical characterizations and biological applications. Chem Rev. 2008;108(6):2064–110.

20. Neuberger T, Schöpf B, Hofmann H, Hofmann M, Von Rechenberg B. Superparamagnetic nanoparticles for biomedical applications: Possibilities and limitations of a new drug delivery system. J Magn Magn Mater. 2005;293(1):483–96.

21. Shaw DJ. Introduction to Colloid & Surface Chemistry. 1966.

22. Zhou L, Zhou Y, Sun Y. Studies on the mechanism and capacity of hydrogen uptake by physisorption-based materials. Int J Hydrogen Energy. 2006;31(2):259–64.

23. Spectronic T. Basic UV-Vis Theory , Concepts and Applications Basic UV-Vis Theory , Concepts and Applications. :1–28.

24. WYATT Technology. The Theory Behind Dynamic Light Scattering (DLS) [Internet]. [cited 2017 Apr 5]. Available from: http://www.wyatt.com/library/theory/dynamic-light-scattering-theory.html

25. Carrassi a, Abati S. [Introduction to scanning electron microscopy]. Mondo Odontostomatol [Internet]. 2007;29(2):29–36. Available from: http://www.ncbi.nlm.nih.gov/pubmed/3313016

26. Fan M, Dai D, Huang B. Fourier Transform - Materials Analysis. Fourier Transform - Mater Anal [Internet]. 2012;45–68. Available from: http://www.intechopen.com/books/fourier-transform-materials-analysis

27. Stuart BH. Infrared Spectroscopy: Fundamentals and Applications [Internet]. Vol. 8, Methods. 2004. 224 p. Available from: http://doi.wiley.com/10.1002/0470011149

28. Sahoo SK, Agarwal K, Singh a K, Polke BG, Raha KC. Characterization of γ- and α-Fe 2 O 3 nano powders synthesized by emulsion precipitation-calcination route and rheological behaviour of α-Fe 2 O 3. Sci Technol. 2010;2(8):118–26.

29. Chaplin M. Water absorption spectrum. 2014;1–8. Available from: http://www1.lsbu.ac.uk/water/vibrat.html

30. Chickos J (UMSL), Garin D (UMSL), D'Souza V (UMSL). IR Spectra. :2. Available from: http://www.umsl.edu/~orglab/

31. Kunz PC, Meyer H, Barthel J, Sollazzo S, Schmidt AM, Janiak C. Metal carbonyls supported on iron oxide nanoparticles to trigger the CO-gasotransmitter release by magnetic heating. Chem Commun (Camb) [Internet]. 2013;49(1997):4896–8. Available from: http://www.ncbi.nlm.nih.gov/pubmed/23609342

32. Park G, Seo D, Chung IS, Song H. Poly(ethylene glycol)- and carboxylate-functionalized gold nanoparticles using polymer linkages: Single-step synthesis, high stability, and plasmonic detection of proteins. Langmuir. 2013;29(44):13518–26.

33. Gref R, Lück M, Quellec P, Marchand M, Dellacherie E, Harnisch S, et al. "Stealth" corona-core nanoparticles surface modified by polyethylene glycol (PEG): Influences of the corona (PEG chain length and surface density) and of the core composition on phagocytic uptake and plasma protein adsorption. Colloids Surfaces B Biointerfaces. 2000;18(3–4):301–13.

34. Amstad E, Textor M, Reimhult E. Stabilization and functionalization of iron oxide nanoparticles for biomedical applications. Nanoscale. 2011;3(7):2819–43.

35. Ben-Shalom N, Pinto R. Natural colloidal particles: the mechanism of the specific interaction between hesperidin and pectin. Carbohydr Polym. 1999;38(2):179–82.

36. Backman A. Zeta Potential Analysis of Nanoparticles. nanoComposix. 2002;(September):23–7.

37. Klein D. Organic Chemistry. Second Edi. John Wiley and Sons, Inc; 2015.

Authors Biography

Banton H. Heithoff was Born in Little Rock, Arkansas on April 11th, 1995. He graduated from Voorhees High School in 2013. Majoring in Bioengineering he expects to graduate May of 2017. He is a member of the Biomedical Engineering society and Engineers without Boarders. After Graduation Banton will start work at Idexx Laboratories.